Bavituximab Decreases Immunosuppressive Myeloid-Derived Suppressor Cells in Newly Diagnosed Glioblastoma Patients

K. Ina Ly[1], Leland G. Richardson[2], Mofei Liu[3], Alona Muzikansky[4], Jonathan Cardona[5], Kevin Lou[5], Andrew L. Beers[5], Ken Chang[5,6], James M. Brown[5], Xiaoyue Ma[5], David A. Reardon[7], Isabel C. Arrillaga-Romany[1], Deborah A. Forst[1], Justin T. Jordan[1], Eudocia Q. Lee[7], Jorg Dietrich[1], Lakshmi Nayak[7], Patrick Y. Wen[7], Ugonma Chukwueke[7], Anita Giobbie-Hurder[3], Bryan D. Choi[2], Tracy T. Batchelor[8], Jayashree Kalpathy-Cramer[5], William T. Curry[2], and Elizabeth R. Gerstner[1,5]

ABSTRACT

Purpose: We evaluated the efficacy of bavituximab—a mAb with anti-angiogenic and immunomodulatory properties—in newly diagnosed patients with glioblastoma (GBM) who also received radiotherapy and temozolomide. Perfusion MRI and myeloid-related gene transcription and inflammatory infiltrates in pre-and post-treatment tumor specimens were studied to evaluate on-target effects (NCT03139916).

Patients and Methods: Thirty-three adults with *IDH*–wild-type GBM received 6 weeks of concurrent chemoradiotherapy, followed by 6 cycles of temozolomide (C1-C6). Bavituximab was given weekly, starting week 1 of chemoradiotherapy, for at least 18 weeks. The primary endpoint was proportion of patients alive at 12 months (OS-12). The null hypothesis would be rejected if OS-12 was ≥72%. Relative cerebral blood flow (rCBF) and vascular permeability (Ktrans) were calculated from perfusion MRIs. Peripheral blood mononuclear cells and tumor tissue were analyzed pre-treatment and at disease progression using RNA transcriptomics and multispectral immunofluorescence for myeloid-derived suppressor cells (MDSC) and macrophages.

Results: The study met its primary endpoint with an OS-12 of 73% (95% confidence interval, 59%–90%). Decreased pre-C1 rCBF (HR, 4.63; $P = 0.029$) and increased pre-C1 Ktrans were associated with improved overall survival (HR, 0.09; $P = 0.005$). Pre-treatment overexpression of myeloid-related genes in tumor tissue was associated with longer survival. Post-treatment tumor specimens contained fewer immunosuppressive MDSCs ($P = 0.01$).

Conclusions: Bavituximab has activity in newly diagnosed GBM and resulted in on-target depletion of intratumoral immunosuppressive MDSCs. Elevated pre-treatment expression of myeloid-related transcripts in GBM may predict response to bavituximab.

Introduction

Median overall survival (OS) in glioblastoma (GBM) is <15 months with standard chemoradiotherapy and adjuvant temozolomide (TMZ; ref. 1). Phosphatidylserine (PS) is a highly immunosuppressive membrane phospholipid on the inner leaflet of the plasma membrane in normal cells. In GBM cells and cells of the tumor microenvironment (including vascular endothelial cells), PS is externalized to the outer leaflet where it is recognized and bound by PS receptors on immune cells (2, 3). This leads to expansion of myeloid-derived suppressor cells (MDSC) and M2-like tumor-associated macrophages (TAM) that promote an immunosuppressive and pro-angiogenic tumor microenvironment (4).

Targeting PS in GBM xenograft models results in tumor cell death (5, 6) and has anti-angiogenic effects (7, 8), thus making it an attractive treatment strategy in GBM where neovascularization is prominent within the tumor microenvironment (9). Furthermore, PS-targeting agents reprogram the tumor microenvironment to an immune-activated state, including decreased MDSCs, TGFβ, and IL10 levels; increased TNFα and IL12 levels; repolarization of TAMs from an M2 to M1 phenotype; and induction of potent adaptive antitumor T-cell immunity (10, 11). In preclinical models, a synergistic effect between PS-targeting agents, radiotherapy, and TMZ has been observed (12, 13).

Bavituximab is a genetically engineered immunoglobulin gamma 1 (IgG1) chimeric mAb that binds β2-glycoprotein-1 (β2-GP1) to form a complex of β2-GP1 with PS, thereby reversing the immunosuppressive effect of PS (14). Bavituximab treatment *in vitro* and *in vivo* resulted in reduced tumor growth and prolonged survival that was enhanced by co-administration of chemotherapy and radiotherapy (3).

In this open-label, single-arm, phase 2 trial (NCT03139916), we evaluated the efficacy of bavituximab given with standard chemoradiotherapy and adjuvant TMZ in newly diagnosed GBM (nGBM). We assessed target-specific impact with serial perfusion MRI and by measuring myeloid-associated gene transcription and myeloid cell infiltrates at various timepoints during treatment to better understand the mechanism of action of bavituximab in GBM.

[1]Stephen E. and Catherine Pappas Center for Neuro-Oncology Massachusetts General Hospital Cancer Center, Boston, Massachusetts. [2]Department of Neurosurgery Massachusetts General Hospital, Boston, Massachusetts. [3]Division of Biostatistics, Department of Data Sciences, Dana-Farber Cancer Institute, Boston, Massachusetts. [4]Department of Biostatistics Massachusetts General Hospital Cancer Center, Boston, Massachusetts. [5]Athinoula A. Martinos Center for Biomedical Imaging, Massachusetts General Hospital, Boston, Massachusetts. [6]Department of Medicine, Memorial Sloan Kettering Cancer Center, New York, New York. [7]Center for Neuro-Oncology, Dana-Farber Cancer Institute, Boston, Massachusetts. [8]Department of Neurology, Brigham and Women's Hospital, Boston, Massachusetts.

W.T. Curry and E.R. Gerstner contributed equally as co-authors of this article.

Corresponding Author: Elizabeth R. Gerstner, Massachusetts General Hospital, 55 Fruit Street, Boston, MA 02114. Phone: 617-724-8770; E-mail: egerstner@mgh.harvard.edu

Clin Cancer Res 2023;29:3017–25

doi: 10.1158/1078-0432.CCR-23-0203

Translational Relevance

In this phase 2 trial, we added bavituximab, an antibody with anti-angiogenic and immunomodulatory properties, to standard radiotherapy and temozolomide in newly diagnosed patients with glioblastoma (GBM). Pre-treatment overexpression of myeloid-related genes in tumor tissue was associated with longer survival and post-treatment tumor specimens contained fewer myeloid-derived suppressor cells (which promote the immunosuppressive GBM microenvironment), suggesting an on-target effect of bavituximab. Seventy-three percent of patients were alive at 12 months, suggesting some efficacy of bavituximab and warranting further study.

Patients and Methods

Patient eligibility

Eligibility criteria included: new diagnosis of histologically confirmed GBM or GBM variant (e.g., gliosarcoma); confirmation of wild-type *IDH* status by IHC or sequencing; age ≥18 years; no prior immunotherapy, alkylating agents, or radiotherapy to the brain; Karnofsky Performance Status (KPS) ≥60; life expectancy >6 months; adequate bone marrow, renal, and liver function; ability to undergo MR imaging; and dexamethasone dose <4 mg daily (or equivalent of another corticosteroid) at treatment initiation. Patients with both non-measurable and measurable disease by RANO criteria at baseline were eligible for inclusion. Exclusion criteria included: receipt of other investigational agents; known allergic reactions to compounds of similar chemical or biologic composition to bavituximab; concurrent use of moderate and/or potent enzyme inducers or inhibitors affecting bavituximab metabolism; uncontrolled intercurrent medical or psychiatric illness and social factors limiting compliance with study requirements; current pregnancy; known history of HIV, hepatitis B and C; history of other active malignancy (excluding *in situ* tumors) in the past 3 years; and known bleeding disorder/coagulopathy. Representativeness of study participants is shown in Supplementary Table S1. The study was conducted in accordance with the U.S. Common Rule.

Study design, treatment, and endpoints

This open-label, single-arm, phase 2 study conducted at the Massachusetts General Hospital and Dana-Farber Cancer Institute (NCT03139916) was approved by the Institutional Review Board of the Dana-Farber/Harvard Cancer Center and conducted in accordance with institutional and federal guidelines for human investigations. All participants were informed of the investigational nature of the study and provided written informed consent before enrollment.

Treatment started at least three weeks after craniotomy or at least two weeks after brain biopsy. Patients received fractionated involved-field radiotherapy (60 Gy, delivered in up to 2 Gy fractions per day) and concurrent TMZ (75 mg/m^2 per day) over 6 weeks, followed by six cycles of monthly adjuvant TMZ (C1-C6; 150–200 mg/m^2 on days 1–5 of each cycle; Supplementary Fig. S1). Bavituximab was given intravenously at 3 mg/kg weekly. This dose was selected on the basis of the data from phase 1 single-agent and phase 2 combination-therapy studies in which combination therapy did not substantially increase the risks of side effects. Bavituximab was administered starting day 5 of radiotherapy, for at least 18 weeks (i.e., until the end of C2), with the option to continue if tolerated. Treatment duration was based on the known synergism between bavituximab, radiotherapy, and TMZ and the diminishing effects of radiotherapy over time. Participants were pre-medicated with intravenous hydrocortisone 250 mg and diphenhydramine 50 mg if needed. To determine whether concurrent steroid treatment (including hydrocortisone pre-medication) interfered with response, patients were grouped by steroid dose during treatment with bavituximab (group 1: low-dose or no steroids; group 2: high-dose steroids; Supplementary Data).

The primary endpoint was proportion of patients alive at 12 months (OS-12). Secondary endpoints included progression-free survival (PFS; defined as time from treatment start to disease progression or death), OS (defined as time from treatment start to death or last follow-up, whichever occurred first), radiographic response, and bavituximab toxicity.

MRI acquisition, processing, and analysis

Patients underwent combined structural and physiologic MR imaging at baseline (pretreatment), pre-C1 TMZ (4 weeks post-chemoradiotherapy), and pre-C3 TMZ if they remained on treatment ("research MRIs"; Supplementary Fig. S1; Supplementary Table S2). Research MRIs included T2SPACE, FLAIR, dynamic contrast enhanced (DCE), dynamic susceptibility contrast (DSC), diffusion tensor imaging (DTI), and pre- and post-contrast T1-weighted MPRAGE images. DSC imaging included gradient echo (GE; reflecting panvascular or both micro- and macrovascular perfusion) and spin echo (SE; reflecting microvascular perfusion) images. After the pre-C3 MRI, patients could continue participation in research MRIs or undergo routine clinical MRIs every two months. Clinical MRIs included high-resolution T1-weighted post-contrast and FLAIR sequences; DTI and DSC imaging were not routinely acquired and therefore not included in the analysis after pre-C3. Response was determined per iRANO criteria by the treating physician (15).

For research scans, structural images (FLAIR, pre-/post-contrast MPRAGE) and parameter maps from DTI, DSC, and DCE imaging were registered to T2SPACE images using the BRAINSFit module in 3D Slicer (16). A deep-learning algorithm was used to segment contrast-enhancing tumor on MPRAGE images (excluding necrotic and hemorrhagic regions) and abnormal FLAIR-hyperintense areas on FLAIR images to generate the contrast-enhancing (CE) and FLAIR tumor regions of interest (ROI), respectively (17). ROIs were reviewed and manually adjusted as needed (K.I. Ly or E.R. Gerstner). Median values for ADC, Ktrans (a measure of vascular permeability), panvascular and microvascular relative cerebral blood volume (rCBV), and relative cerebral blood flow (rCBF) were calculated from contrast-enhancing and FLAIR-hyperintense ROIs. Ktrans maps (reflecting vascular permeability) were generated from DCE imaging. The detailed protocols for acquisition and post-processing steps for research scans are found under Supplementary Data.

Peripheral blood and tumor tissue collection and processing

Peripheral blood was collected pre-treatment, during week 6 of chemoradiotherapy, first week post-chemoradiotherapy, and monthly for two months during adjuvant TMZ/bavituximab (Supplementary Data).

Tumor tissue was obtained at diagnosis and progression (if available) and processed per standard pathology protocol. Analysis was performed on formalin-fixed paraffin-embedded (FFPE) tissue.

Gene expression profiling and analysis

RNA was extracted from peripheral blood mononuclear cell (PBMC) lysates and FFPE tumor tissue using the Qiagen RNeasy

Mini Kit (Qiagen; 74134). Quality and abundance of isolated RNA was measured using the Aligent Bioanalyzer 2100 and NanoDrop 2000 before sequencing. The nCounter Myeloid Innate Immunity Panel (probing for 770 myeloid-associated genes) was used to analyze their expression in PBMCs and tumor tissue (NanoString Technologies; ref. 18). All raw data were reviewed for quality using the nCounter Advanced Analysis 2.0 software (NanoString Technologies). Sequencing results were uploaded to ROSALIND (https://rosalind.onramp.bio/) for analysis and plot visualization (ROSALIND Inc.). Normalization, fold changes, and *P* values were calculated on ROSALIND using criteria from the nCounter Advanced Analysis 2.0 protocol. Cutoff values for *P* value and fold change were 0.05 and +1.5/−1.5, respectively. We entered Nanostring-derived gene expression data into Metascape (19), an open-access resource (www.metascape.org) that provides expression analysis and defines over-represented gene sets, or "enrichment clusters."

Immunofluorescence staining and image acquisition and quantification

FFPE blocks with tumor cell percentages >80% were selected before sectioning. Slides were stained for intratumoral myeloid cellular infiltrate, focusing on the number of TAMs and MDSCs (Supplementary Data). Slides were scanned using the Vectra Polaris microscope and unmixed with inForm software (Akoya Biosciences), incorporating the algorithm generated by a spectral library using single-fluorophore label control slides. Unmixed images for each slide were fused and uploaded to the Halo software (Indica Labs) for analysis. The entire tumor tissue area was manually annotated, excluding folds or debris. Cell segmentation and staining intensity thresholds were assigned by a blinded individual. Parameters defining each cell type were applied to the analysis algorithm to each slide. M1 or M2 TAMs were identified on the basis of co-staining for CD68 and CD163 ($CD68^+CD163^-$: M1 TAMs, $CD68^+CD163^+$: M2 TAMs). Granulocytic MDSCs were characterized by co-staining with CD15 and Lox-1 (a differentiation marker for human MDSCs; refs. 20, 21). Positive cell counts were measured as number of positive cells per mm^2 of tissue.

Statistical analysis

All statistical analyses (except for the immune marker analysis) were performed using SAS9.4 (SAS Institute Inc.). OS-12 in recent studies of novel agents in nGBM was 60%–68% (22, 23). This study was designed to compare OS-12 against a historic control of 60% using the method of Brookmeyer and Crowley (24). A sample of 33 patients would provide 0.88 power (target = 0.85) to detect OS-12 of 80%, given a one-sided alpha of 0.09 (target = 0.1). The null hypothesis would be rejected if the observed Kaplan–Meier estimate of OS-12 was ≥72%. To allow for early patient drop-out or withdrawal, 36 patients were enrolled. Patients lost to follow-up before documented progression or death were censored at the time of their last visit.

The relationship of clinical (*MGMT* status, age, steroid group) and imaging markers with OS-12 was tested using univariate logistic regression. The correlation between markers and PFS/OS was tested using Cox proportional hazards model. For the multivariate analysis, three imaging markers (which were significant in univariate analyses and of clinical relevance) were included after excluding high correlation between markers (using Pearson correlation coefficient). To assess the association of changes in imaging markers with OS-12, PFS, and OS, we calculated the fold-change between pre-C1 and baseline (fold change = timepoint/baseline). Values were dichotomized into "low" versus "high" at the median of their distribution to ensure an unbiased division and equal number of patients in each group. No adjustment was made for multiple testing, given that these were exploratory and hypothesis-generating analyses.

For the immune marker analysis, GraphPad Prism 9.1 software was used for statistical analyses and visualization. We categorized patients into "low" and "high" PFS/OS groups, divided at the median. All tests were two-sided with a *P* value of <0.05 considered statistically significant. We used unpaired *t* and Mann–Whitney *U* tests to assess differences between timepoints.

Data availability

The data generated in this study may be available upon request from the corresponding author.

Results

Patient characteristics

Thirty-six patients with *IDH*-wt nGBM were enrolled between July 2017 and 2018 (**Table 1**). Of these, 33 patients were evaluable; 2 were not evaluable because of withdrawal of consent and 1 experienced clinical progression before start of treatment. Median age was 59 years and median KPS was 90. Fifty-eight percent of tumors were *MGMT* promoter-unmethylated. Fifteen patients (45.5%) did not require dexamethasone at treatment initiation and during treatment. Ten patients (30.3%) required low-dose or no steroids and 23 patients (69.7%) required high-dose steroids during treatment. Six (18.2%) patients had a biopsy, 12 (36.4%) patients underwent a subtotal resection, and 15 (45.5%) patients had a gross total or near–gross total resection (Supplementary Data).

Table 1. Patient characteristics and outcomes.

Patient characteristics	*n* = 33
Median age (y, range)	59 (24–75)
Median KPS (range)	90 (70–100)
Gender	
Female	17 (51.5%)
Male	16 (48.5%)
Race	
Black or African American	1 (3.0%)
White	32 (97.0%)
Extent of resection	
Biopsy	6 (18.2%)
Subtotal resection	12 (36.4%)
Gross total or near–gross total resection	15 (45.5%)
MGMT promoter methylation status	
Methylated	12 (36.4%)
Unmethylated	19 (57.6%)
N/A	2 (6.1%)
Outcomes	
OS-12	72.7%
Median PFS in months (95% CI)	6.9 (6.2–9.7)
Median OS in months (95% CI)	15.4 (13.3–23.6)
Best radiographic response[a]	
Complete response	0/26 (0%)
Partial response	4/26 (15.4%)
Stable disease	26/33 (78.8%)
Progressive disease	3/33 (9%)

[a]Denominator varies because only patients with measurable disease can achieve a complete or partial response.

Clinical and radiographic outcomes

The proportion of patients alive at 12 months (OS-12) was 72.7% [95% confidence interval (CI), 59%–90%; 24 patients alive at 12 months], achieving the study's primary endpoint. At the time of data cutoff (May 2021), median PFS and OS were 6.9 and 15.4 months, respectively (Supplementary Fig. S2). Thirty (90.1%) patients progressed. Of 3 patients without disease progression, one died of aspiration pneumonia, one is still on trial, and one has been lost to follow-up. Twenty-eight (84.8%) patients have died, 4 are alive, and one has been lost to follow-up. Twenty-six of 33 patients (78.8%) had measurable disease at baseline per RANO criteria. Stable disease was observed in 79%, partial response in 15%, and progressive disease in 9% of patients. In those with a partial response, the median duration of response was 177 days (range, 55–225 days; Supplementary Fig. S3). Methylated *MGMT* status was associated with improved PFS ($P = 0.003$) and OS ($P = 0.002$) but age and steroid use were not (Supplementary Table S3).

Safety

The median number of bavituximab doses given was 24 (range, 5–85). Five patients stopped after a median of 18 doses (range, 6–28) due to personal preference. One patient stopped after 14 doses due to repeated hypersensitivity reactions (facial flushing, nausea) despite standard pre-medication.

Twenty-eight (84.8%) patients had adverse events (AE) that were possibly, probably, or definitely related to bavituximab. AEs observed in at least 10% of patients are shown in Supplementary Table S4. Nine AEs in five patients resulted in interruption of treatment with bavituximab (Supplementary Table S5). In one patient with grade 2 fatigue thought to be possibly related to radiotherapy, treatment was permanently discontinued. Four grade 3 or 4 AEs and no grade 5 were reported.

Physiological imaging analysis

On univariate analysis, high baseline CE volume, FLAIR volume, panvascular and microvascular rCBV, panvascular rCBF, and Ktrans in the CE region were associated with worse OS (**Table 2**). There was a trend toward significance for Ktrans and OS-12 (OR, 9.33; 95% CI, 0.96–90.94; $P = 0.054$). High baseline panvascular rCBV and Ktrans within the CE region were predictive of worse PFS. On multivariate analysis, we stratified patients by *MGMT* status and included CE volume and panvascular rCBV as predictors, given that these are known biologic markers of tumor aggressiveness and vascularity. CE volume remained associated with worse OS ($P = 0.04$). A trend was also observed between high panvascular rCBV and worse OS ($P = 0.064$). High panvascular rCBV remained a negative predictor of PFS ($P = 0.047$).

At the pre-C1 timepoint, the fold-change of imaging markers compared with baseline was analyzed (**Fig. 1**; Supplementary Table S6). The median fold-change in panvascular rCBF was 0.76. Patients with a fold-change ≥0.76 had a three times greater risk of death compared with those with a fold change <0.76 ($P = 0.018$; **Table 2**). For Ktrans, the median fold-change was 1.34. Patients with a fold-change ≥1.34 had an 83% reduction in the hazard of death compared with those with a fold change <1.34 ($P = 0.003$; **Table 2**). On multivariate analysis stratified by *MGMT* status, both markers remained significant: a pre-C1 increase or stable panvascular rCBF predicted worse OS whereas increased Ktrans was associated with a reduction in death (Supplementary Fig. S4). At the pre-C3 timepoint, the fold-change of imaging markers was not associated with OS-12, OS, or PFS on univariate analysis.

Table 2. Correlation between tumor imaging biomarkers at the baseline and pre-C1 timepoints and PFS and OS based on univariate and multivariate analysis.

	PFS		OS	
Imaging marker	**HR (high vs. low; 95% CI)**	***P***	**HR (high vs. low; 95% CI)**	***P***
Univariate analysis				
Baseline				
CE volume	1.90 (0.89–4.09)	0.099	3.25 (1.40–7.56)	**0.006**
FLAIR volume	1.60 (0.75–3.42)	0.229	2.72 (1.22–6.07)	**0.014**
Pan rCBF (CE)	2.16 (0.99–4.71)	0.053	2.60 (1.16–5.84)	**0.02**
Pan rCBV (CE)	2.26 (1.03–4.94)	**0.041**	3.11 (1.35–7.15)	**0.008**
Micro rCBV (CE)	1.77 (0.81–3.83)	0.15	2.35 (1.07–5.18)	**0.034**
Ktrans (CE)	2.49 (1.12–5.55)	**0.025**	4.18 (1.77–9.87)	**0.001**
Fold-change at pre-C1 timepoint				
Pan rCBF (CE)	2.16 (0.95–4.93)	0.067	2.92 (1.20–7.10)	**0.018**
Ktrans (CE)	0.39 (0.14–1.05)	0.062	0.17 (0.05–0.55)	**0.003**
Multivariate analysis				
Baseline				
CE volume	1.39 (0.51–3.79)	0.52	3.72 (1.06–13.08)	**0.04**
Pan rCBV (CE)	2.99 (1.02–8.78)	**0.047**	3.11 (0.94–10.30)	0.064
Fold-change at pre-C1 timepoint				
Pan rCBF (CE)	2.47 (0.81–7.57)	0.113	4.63 (1.17–18.37)	**0.029**
Ktrans (CE)	0.34 (0.09–1.23)	0.1	0.09 (0.02–0.48)	**0.005**

Note: Except for FLAIR volume, all imaging markers were derived from contrast-enhancing (CE) regions of interest (ROI). The median was used to separate patients into "high" and "low" imaging biomarker groups. The hazard ratio (HR) reflects the hazard of death in the "high" compared with the "low" group. For the univariate analysis, only MRI biomarkers with *P* values of <0.05 are shown. See Supplementary Table S4 for univariate analysis of all MRI biomarkers. Pan, panvascular; Micro, microvascular.

Analysis of myeloid-related RNA transcripts in GBM tissue and PBMCs

We performed gene expression profiling and analysis of tumor specimens and PBMCs. At baseline (pre-treatment), RNA analysis of tumor specimens ($n = 10$) showed significantly positive shifts in myeloid-related gene expression in patients with longer survival, with enrichment of 116 and 120 transcripts and downregulation of 1 and 2 gene(s), in patients with longer PFS and OS, respectively (**Fig. 2A–C**). Using Metascape cluster enrichment analysis of overexpressed genes, the most significantly upregulated networks in longer surviving patients were associated with inflammatory response, cytokine signaling, and leukocyte activation (**Fig. 2B–D**).

In comparison, PBMC gene expression data from 26 patients at baseline showed little differential transcription of myeloid-related genes based on survival. Eleven and 18 genes were differentially expressed in high versus low PFS and OS groups, respectively. Approximately equal numbers were upregulated or downregulated (Supplementary Fig. S5).

We also compared RNA transcripts from tumor specimens at diagnosis ($n = 10$) and at progression ($n = 7$), including paired samples (pre- and post-treatment) from 2 patients. Sixty-seven myeloid-related genes were differentially expressed between these two timepoints: 35 and 32 genes were upregulated and downregulated, respectively, at progression (**Fig. 3A**). Metascape cluster enrichment analysis of differentially expressed genes (**Fig. 3B**) revealed that the most commonly upregulated and downregulated functional networks included shifts in expression of IL4, IL10, and IL13, all of which are associated with MDSC maturation and signaling (25).

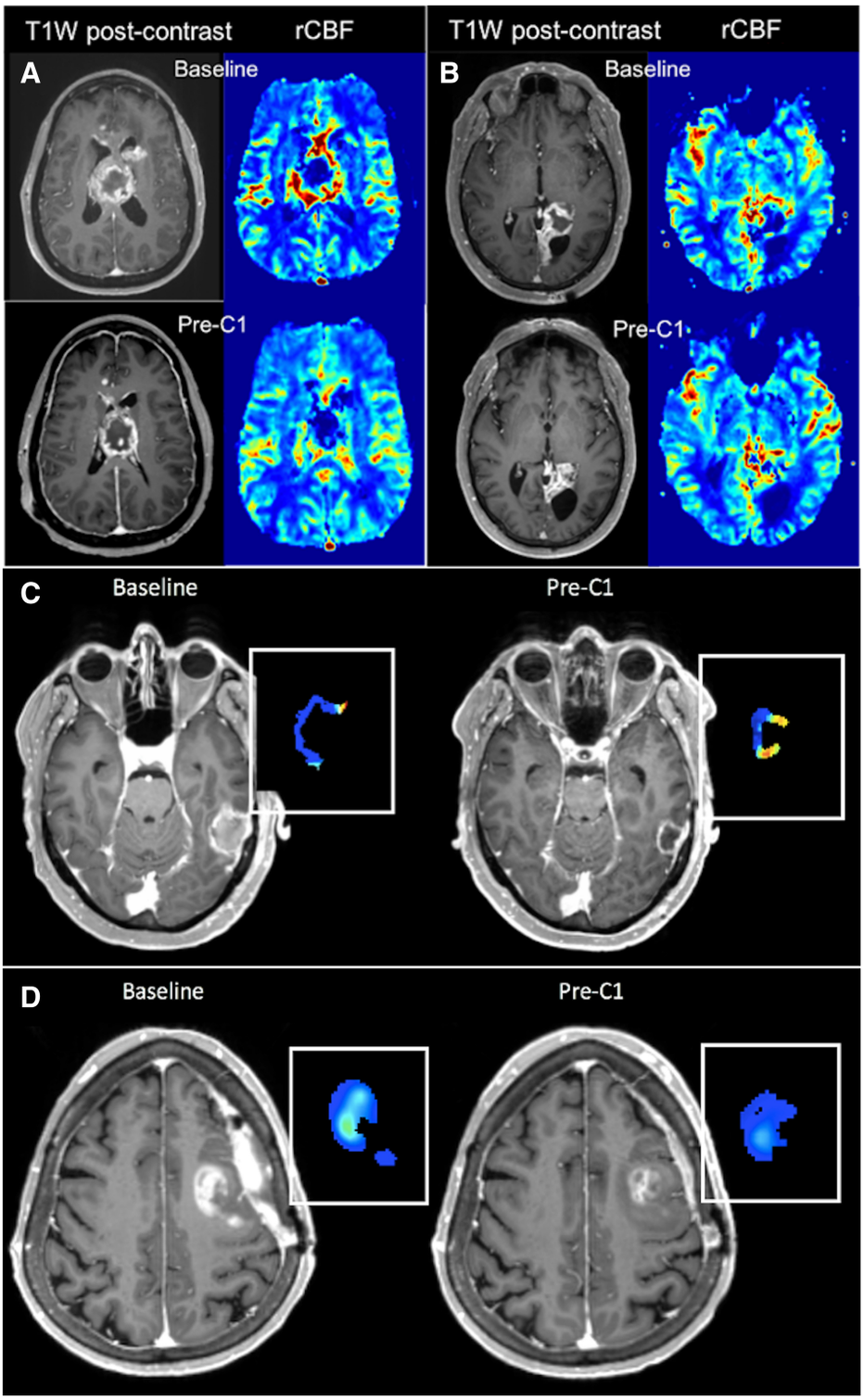

Figure 1.

Examples of association between panvascular rCBF and OS (**A** and **B**) and Ktrans and OS (**C** and **D**). Panvascular rCBF and Ktrans were measured within the contrast-enhancing tumor ROI. **A,** BAV_11 had a decrease in rCBF by 31% (fold-change 0.69) at the pre-C1 timepoint and had an OS of 23.9 months, which was significantly longer than the median OS of 15.4 months. **B,** BAV_17 had an increase in rCBF by 54% (fold-change 1.54) at the pre-C1 timepoint and had an OS of only 11.3 months. **C,** BAV_33 had a 1.8-fold increase in pre-C1 vascular permeability (as measured by Ktrans) compared with baseline and had an OS of 26.7 months. **D,** BAV_09 experienced a decrease of 34.5% (0.65-fold change) in pre-C1 vascular permeability at the pre-C1 timepoint; OS was 14.7 months. Pop out in **C** and **D** represents Ktrans map within the contrast-enhancing tumor.

Multispectral immunofluorescence

We performed multispectral immunofluorescence to characterize the phenotype of TAMs in tumor tissue at diagnosis ($n = 10$) or progression ($n = 8$). There was no difference in the density of TAMs or M2/M1 ratio in tumor tissue between these timepoints (Supplementary Fig. S6). However, we found decreased MDSCs in tumor tissue after bavituximab treatment (4.5+2.3 cells/mm^2) compared with time of diagnosis (63.1+4.5 cells/mm^2; **Fig. 4**; Supplementary Fig. S7).

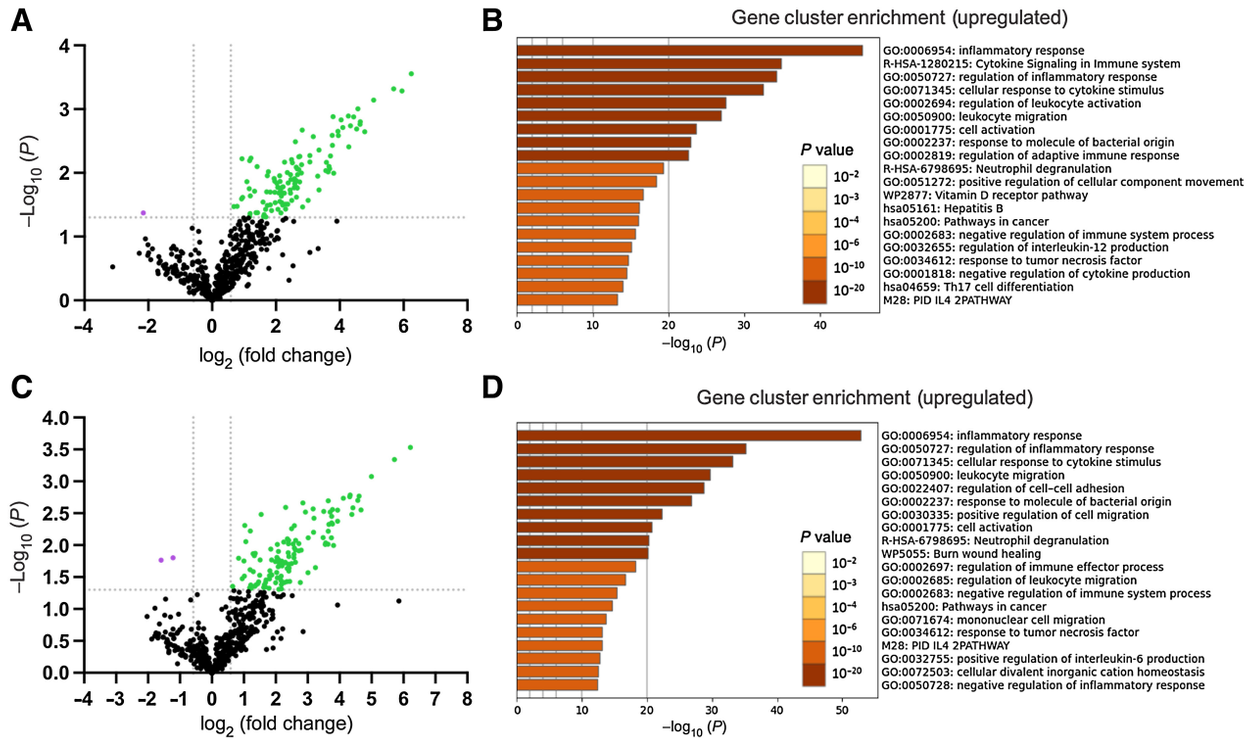

Figure 2.

Enhanced PFS and OS after bavituximab, chemoradiotherapy, and adjuvant TMZ are associated with differential expression of myeloid-related genes in tissue obtained at time of diagnosis. **A,** Volcano plot demonstrating that 116 myeloid-related genes (green dots) were significantly more highly expressed in the tumors of patients that had greater-than-median PFS. **C,** Volcano plot demonstrating that 120 myeloid-related genes (green dots) were significantly more highly expressed in tumors of patients that had greater-than-median OS. **B** and **D,** Metascape cluster enrichment analysis revealed upregulated baseline expression of networks associated with inflammatory responses, cellular responses to cytokine stimulus, leukocyte migration, and others listed in the figure.

Discussion

We evaluated the efficacy of bavituximab with standard chemoradiotherapy and adjuvant TMZ in 33 patients with *IDH*–wild-type nGBM. The study met its primary endpoint with an OS-12 of 72.7%. However, median PFS (6.9 months) and OS (15.4 months) were comparable with standard treatment in combined methylated and unmethylated patients with GBM (1). Bavituximab was well tolerated and not associated with significant AEs. Among current clinical reports of bavituximab in cancer (26–29), our study is the first to directly and prospectively probe tumor microenvironment and assess on-target effects of bavituximab using perfusion MRI and expression of immune-related genes and relevant immune cell subsets.

Baseline elevation and interval increase or stable panvascular rCBF were associated with decreased survival, consistent with previous studies in nGBM (30, 31). Whereas these studies found that a pre-C1 *decrease* in vascular permeability (measured by Ktrans) was associated with improved survival, we found that an *increase* in Ktrans was associated with improved outcome. This may suggest a greater immune response causing breakdown of the blood–brain barrier and, consequently, better penetration of bavituximab to achieve on-target effects within the tumor microenvironment.

The GBM immune microenvironment is characterized by relatively few $CD8^+$ T cells and abundant macrophages (32). M2 TAMs, the predominant cells in the GBM microenvironment, promote immune tolerance (33). Cellular interactions in this M2-skewed microenvironment enhance MDSC differentiation that further inhibit antigen-specific T-cell responses. In animal models, bavituximab-mediated PS blockade leads to reprogramming of TAMs from an immunosuppressive M2 phenotype to an immune-active M1 phenotype and reduces MDSCs (3, 14), with the latter phenomenon confirmed in patients with GBM in this study. Furthermore, our finding that myeloid transcripts were more highly expressed in tumors from patients with better survival supports that bavituximab might have greater activity when the drug's targets are enriched. In GBM subsets, increased macrophage and microglia infiltration has been associated with worse survival (34). As expected, expression levels of myeloid-related genes in PBMCs did not predict survival as bavituximab exerts its impact within the tumor microenvironment and not in PBMCs. Accordingly, we found that MDSC number in tumor specimens was reduced at time of progression, confirming an on-target, intratumoral effect of bavituximab and a potential step forward in the modulation of the GBM immune microenvironment.

Our study has some limitations. The single-arm design does not permit evaluation of the differential effects of bavituximab and standard therapy on immune cell modulation and 6/30 patients discontinued treatment, although this was less than with other bavituximab studies. Tumor specimens were obtained from only 21% of patients at progression so may not be representative of the entire cohort or accurately reflect the tumor microenvironment during treatment. However, GBM progression is typically associated with at

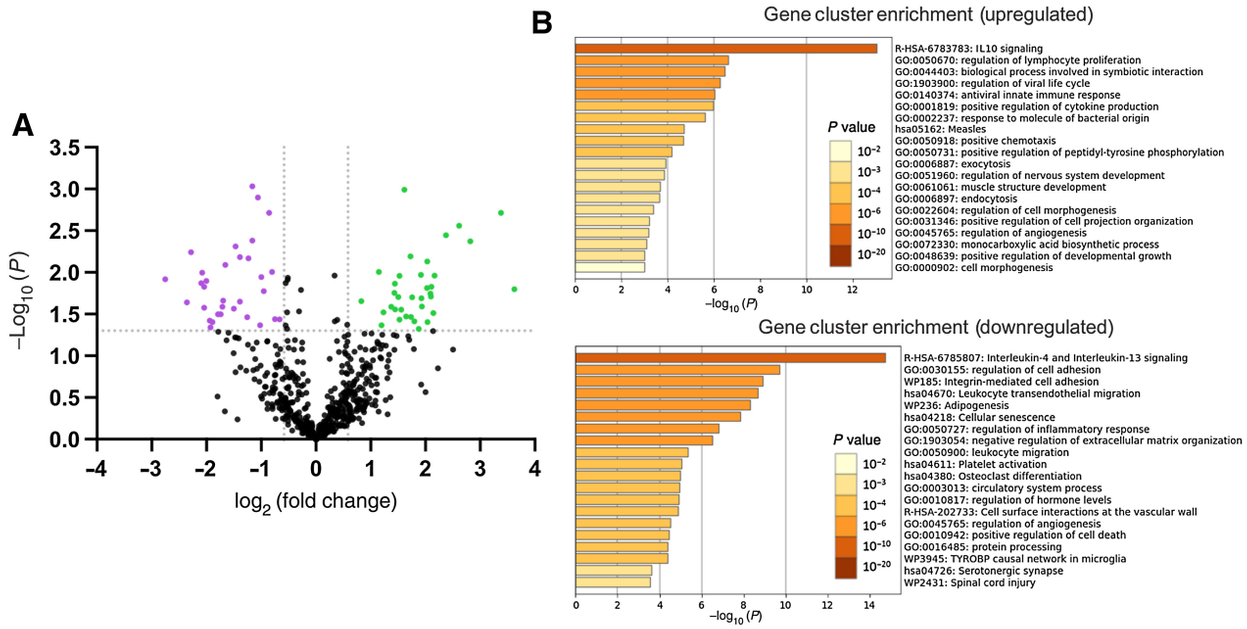

Figure 3.
Myeloid-related genes and functional networks are differentially expressed in glioblastoma tissue obtained at diagnosis and at progression after treatment with chemoradiotherapy and bavituximab. **A,** Volcano plot (green dots represent 35 significantly upregulated genes, purple represent 32 significantly downregulated genes). **B**, Metascape cluster enrichment analysis details both the upregulation and downregulation of myeloid-related processes after treatment.

least maintained, if not greater, local immunosuppression and increased numbers of M2-TAMs and MDSCs (35). Therefore, our finding of decreased MDSCs at progression likely reflects on-target treatment effects, and tumor progression presumably occurred because of molecular and/or immune escape. Bavituximab typically suppresses IL10 expression so our finding that IL10 was upregulated at progression suggests an immune escape process. A "window of opportunity" trial focusing on changes in TAMs, MDSCs, and lymphocyte subsets during bavituximab treatment might clarify peak immune changes associated with this drug (32, 36). Our target OS-12 was generated from historical controls and was a conservative target because we enrolled both MGMT methylated and unmethylated patients that are now known to have distinct prognoses. However, for this first-in-GBM study, we believed this was a reasonable initial target endpoint.

In summary, this mechanistically driven phase 2 trial is the first to demonstrate on-target effects of bavituximab with a decrease in

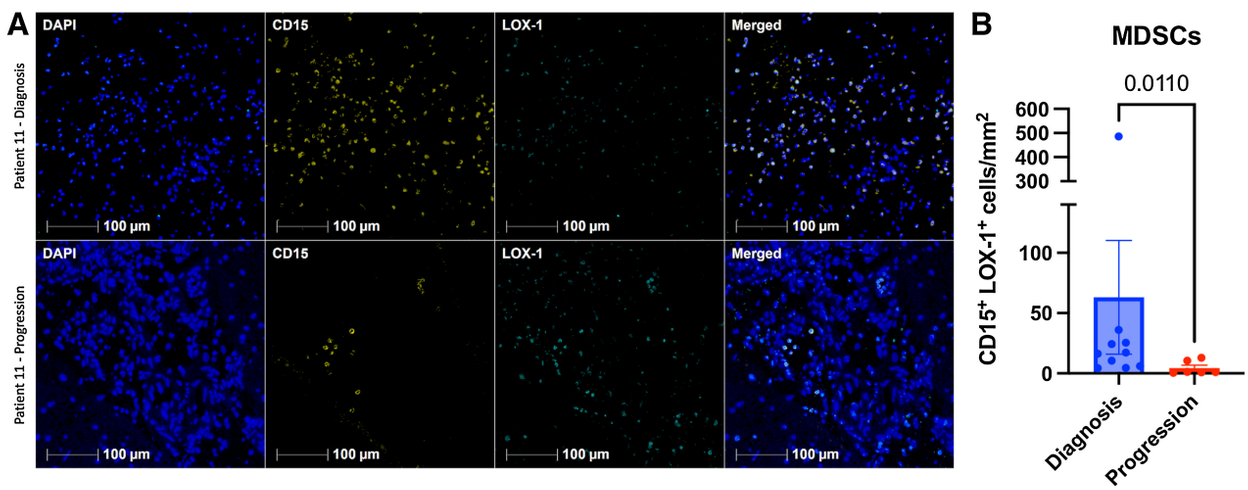

Figure 4.
Immunofluorescence of infiltrating MDSCs in the tumor microenvironment before and after bavituximab treatment. **A,** Representative immunofluorescence images of infiltrating MDSCs in a matched-pair tumor sample before (top row) and after (bottom row) bavituximab treatment. Specimens were labeled with antibodies against DAPI (blue), CD15 (yellow), and LOX-1 (aqua). **B,** The number of MDSCs was significantly reduced in specimens collected at the time of progression compared with initial diagnosis. A *P* value is shown above the brackets.

intratumoral MDSCs. Greater expression of myeloid transcripts in pre-treatment tumor tissue correlated with PFS and OS. Further study is warranted to identify those most likely to benefit from bavituximab and optimal combination therapies. Higher serum β2-GP1 levels have been explored as a marker of response in patients with non-squamous non–small cell lung cancer (NSCLC; ref. 26) but further validation of β2-GP1 levels as a predictive biomarker will be required. In addition, in a phase 3 trial of non-squamous NSCLC, *post hoc* analyses revealed that OS was improved in a small subset of patients who received immune checkpoint inhibition after docetaxel and bavituximab (26). As a result, several trials of bavituximab and pembrolizumab in solid cancers are ongoing (NCT04099641, NCT03519997, and NCT04150900). In GBM, pembrolizumab monotherapy or combined with bevacizumab has shown limited benefit. However, on the basis of the above data, a potential next step in GBM is to combine bavituximab with checkpoint inhibition or other immune-activating approaches such as vaccination or chimeric antigen receptor T-cell therapy to maximize the intratumoral immune response.

Authors' Disclosures

D.A. Reardon reports personal fees from Agios, AnHeart Therapeutics, Avita Biomedical, Inc., Bristol Myers Squibb, Boston Biomedical, CureVac AG, Del Mar Pharma, DNAtrix, Hoffman-LaRoche, Ltd., Imvax, Janssen, Kiyatec, Medicenna Therapeutics, Neuvogen, Novartis, Novocure, Pyramid Biosciences, Sumitomo Dainippon Pharma, Vivacitas Oncology, Y-Mab Therapeutics, and Blue Rock Therapeutics outside the submitted work. I.C. Arrillaga-Romany reports grants from NCCN during the conduct of the study; I.C. Arrillaga-Romany also reports personal fees from Boehringer Ingelheim, as well as other support from Astex Pharmaceutical and GSK outside the submitted work. D.A. Forst reports other support from Eli Lilly outside the submitted work. J.T. Jordan reports personal fees from Navio Theragnostics, Alexion Pharmaceuticals, Recursion Pharmaceuticals, Shepherd Therapeutics, and CEC Oncology outside the submitted work. J. Dietrich reports personal fees from Unum Therapeutics and Amgen outside the submitted work. L. Nayak reports grants from Leukemia and Lymphoma Society; personal fees from Ono, BraveBio, and Genmab; and non-financial support and other support from Merck, AstraZeneca, Kazia, and Bristol Myers Squibb outside the submitted work. T.T. Batchelor reports grants from National Institutes of Health outside the submitted work. J. Kalpathy-Cramer reports grants from GE Heathcare and Genentech, as well as other support from Siloam Vision Inc. outside the submitted work. E.R. Gerstner reports grants from NCCN during the conduct of the study. No disclosures were reported by the other authors.

Authors' Contributions

K.I. Ly: Data curation, formal analysis, investigation, visualization, writing–original draft, writing–review and editing. **L.G. Richardson:** Formal analysis, investigation, visualization, writing–original draft, writing–review and editing. **M. Liu:** Formal analysis, writing–original draft, writing–review and editing. **A. Muzikansky:** Conceptualization, formal analysis, writing–review and editing. **J. Cardona:** Investigation. **K. Lou:** Formal analysis, investigation. **A.L. Beers:** Investigation. **K. Chang:** Investigation. **J.M. Brown:** Investigation. **X. Ma:** Investigation. **D.A. Reardon:** Investigation, writing–review and editing. **I.C. Arrillaga-Romany:** Investigation, writing–review and editing. **D.A. Forst:** Investigation, writing–review and editing. **J.T. Jordan:** Investigation, writing–review and editing. **E.Q. Lee:** Investigation, writing–review and editing. **J. Dietrich:** Investigation, writing–review and editing. **L. Nayak:** Investigation, writing–review and editing. **P.Y. Wen:** Investigation, writing–review and editing. **U. Chukwueke:** Investigation, writing–review and editing. **A. Giobbie-Hurder:** Formal analysis, writing–review and editing. **B.D. Choi:** Investigation. **T.T. Batchelor:** Investigation. **J. Kalpathy-Cramer:** Investigation. **W.T. Curry:** Conceptualization, investigation, writing–original draft, writing–review and editing. **E.R. Gerstner:** Conceptualization, funding acquisition, investigation, visualization, writing–original draft, project administration, writing–review and editing.

Acknowledgments

This study was funded by the National Comprehensive Cancer Network Oncology Research Program and from general research support from Oncologie, Inc. (E.R. Gerstner). In addition, funding was provided by A Shot for Life (https://www.ashotforlife.org/) and The Jenny Fund (https://www.thejennyfund.org/; to W.T. Curry).

The publication costs of this article were defrayed in part by the payment of publication fees. Therefore, and solely to indicate this fact, this article is hereby marked "advertisement" in accordance with 18 USC section 1734.

Note

Supplementary data for this article are available at Clinical Cancer Research Online (http://clincancerres.aacrjournals.org/).

Received January 20, 2023; revised March 29, 2023; accepted June 13, 2023; published first June 16, 2023.

References

1. Stupp R, Mason WP, van den Bent MJ, Weller M, Fisher B, Taphoorn MJB, et al. Radiotherapy plus concomitant and adjuvant temozolomide for glioblastoma. N Engl J Med 2005;352:987–96.
2. Birge RB, Boeltz S, Kumar S, Carlson J, Wanderley J, Calianese D, et al. Phosphatidylserine is a global immunosuppressive signal in efferocytosis, infectious disease, and cancer. Cell Death Differ 2016;23:962–78.
3. He J, Yin Y, Luster TA, Watkins L, Thorpe PE. Antiphosphatidylserine antibody combined with irradiation damages tumor blood vessels and induces tumor immunity in a rat model of glioblastoma. Clin Cancer Res 2009;15:6871–80.
4. Beury DW, Parker KH, Nyandjo M, Sinha P, Carter KA, Ostrand-Rosenberg S. Cross-talk among myeloid-derived suppressor cells, macrophages, and tumor cells impacts the inflammatory milieu of solid tumors. J Leukoc Biol 2014;96:1109–18.
5. Blanco VM, Chu Z, Vallabhapurapu SD, Sulaiman MK, Kendler A, Rixe O, et al. Phosphatidylserine-selective targeting and anticancer effects of SapC-DOPS nanovesicles on brain tumors. Oncotarget 2014;5:7105–18.
6. Blanco VM, Curry R, Qi X. SapC-DOPS nanovesicles: a novel targeted agent for the imaging and treatment of glioblastoma. Oncoscience 2015;2:102–10.
7. Wojton J, Chu Z, Mathsyaraja H, Meisen WH, Denton N, Kwon C-H, et al. Systemic delivery of SapC-DOPS has antiangiogenic and antitumor effects against glioblastoma. Mol Ther 2013;21:1517–25.
8. Ran S, He J, Huang X, Soares M, Scothorn D, Thorpe PE. Antitumor effects of a monoclonal antibody that binds anionic phospholipids on the surface of tumor blood vessels in mice. Clin Cancer Res 2005;11:1551–62.
9. Louis DN, Perry A, Wesseling P, Brat DJ, Cree IA, Figarella-Branger D, et al. The 2021 WHO classification of tumors of the central nervous system: a summary. Neuro Oncol 2021;23:1231–51.
10. Denekamp J. Review article: angiogenesis, neovascular proliferation and vascular pathophysiology as targets for cancer therapy. Br J Radiol 1993;66:181–96.
11. Burrows FJ, Thorpe PE. Vascular targeting—a new approach to the therapy of solid tumors. Pharmacol Ther 1994;64:155–74.
12. Hussain N, Davis H, Vallabhapurapu S, Chu Z, Blanco V, Qi X. ATPS-35radiation treatment increases phosphatidylserine externalization on glioblastoma cells—indicates potential target for therapy. Neuro-oncol 2015;17:v25–6.
13. Wojton J, Meisen WH, Jacob NK, Thorne AH, Hardcastle J, Denton N, et al. SapC-DOPS–induced lysosomal cell death synergizes with TMZ in glioblastoma. Oncotarget 2014;5:9703–9.
14. Yin Y, Huang X, Lynn KD, Thorpe PE. Phosphatidylserine-targeting antibody induces M1 macrophage polarization and promotes myeloid-derived suppressor cell differentiation. Cancer Immunol Res 2013;1:256–68.
15. Okada H, Weller M, Huang R, Finocchiaro G, Gilbert MR, Wick W, et al. Immunotherapy response assessment in neuro-oncology: a report of the RANO working group. Lancet Oncol 2015;16:e534–42.
16. Fedorov A, Beichel R, Kalpathy-Cramer J, Finet J, Fillion-Robin J-C, Pujol S, et al. 3D Slicer as an image computing platform for the quantitative imaging network. Magn Reson Imaging 2012;30:1323–41.
17. Beers A, Brown J, Chang K, Hoebel K, Patel J, Ly KI, et al. DeepNeuro: an open-source deep learning toolbox for neuroimaging. Neuroinformatics 2021;19:127–40.

18. Alban TJ, Bayik D, Otvos B, Rabljenovic A, Leng L, Jia-Shiun L, et al. Glioblastoma myeloid-derived suppressor cell subsets express differential macrophage migration inhibitory factor receptor profiles that can be targeted to reduce immune suppression. Front Immunol 2020;11:1191.
19. Zhou Y, Zhou B, Pache L, Chang M, Khodabakhshi AH, Tanaseichuk O, et al. Metascape provides a biologist-oriented resource for the analysis of systems-level datasets. Nat Commun 2019;10:1523.
20. Chai E, Zhang L, Li C. LOX-1^{+} PMN-MDSC enhances immune suppression which promotes glioblastoma multiforme progression. Cancer Manag Res 2019; 11:7307–15.
21. Condamine T, Dominguez GA, Youn J-I, Kossenkov AV, Mony S, Alicea-Torres K, et al. Lectin-type oxidized LDL receptor-1 distinguishes population of human polymorphonuclear myeloid-derived suppressor cells in cancer patients. Sci Immunol 2016;1:aaf8943.
22. Gilbert MR, Dignam JJ, Armstrong TS, Wefel JS, Blumenthal DT, Vogelbaum MA, et al. A randomized trial of bevacizumab for newly diagnosed glioblastoma. N Engl J Med 2014;370:699–708.
23. Lee EQ, Kaley TJ, Duda DG, Schiff D, Lassman AB, Wong ET, et al. A multicenter, phase II, randomized, noncomparative clinical trial of radiation and temozolomide with or without vandetanib in newly diagnosed glioblastoma patients. Clin Cancer Res 2015;21:3610–8.
24. Brookmeyer R, Crowley JJ. A confidence interval for the medial survival time Biometrics 1982;38:29–41.
25. Zhao Y, Wu T, Shao S, Shi B, Zhao Y. Phenotype, development, and biological function of myeloid-derived suppressor cells. Oncoimmunology 2016;5:e1004983.
26. Gerber DE, Horn L, Boyer M, Sanborn R, Natale R, Palmero R, et al. Randomized phase III study of docetaxel plus bavituximab in previously treated advanced non-squamous non–small cell lung cancer. Ann Oncol 2018;29:1548–53.
27. Gerber DE, Spigel DR, Giorgadze D, Shtivelband M, Ponomarova OV, Shan JS, et al. Docetaxel combined with bavituximab in previously treated, advanced nonsquamous non–small cell lung cancer. Clin Lung Cancer 2016;17:169–76.
28. Mokdad AA, Zhu H, Beg MS, Arriaga Y, Dowell JE, Singal AG, et al. Efficacy and safety of bavituximab in combination with sorafenib in advanced hepatocellular carcinoma: a single-arm, open-label, phase II clinical trial. Target Oncol 2019;14: 541–50.
29. Chalasani P, Marron M, Roe D, Clarke K, Iannone M, Livingston RB, et al. A phase I clinical trial of bavituximab and paclitaxel in patients with HER2 negative metastatic breast cancer. Cancer Med 2015;4:1051–9.
30. Ly KI, Vakulenko-Lagun B, Emblem KE, Ou Y, Da X, Betensky RA, et al. Publisher correction: probing tumor microenvironment in patients with newly diagnosed glioblastoma during chemoradiation and adjuvant temozolomide with functional MRI. Sci Rep 2019;9:8721.
31. Gerstner ER, Zhang Z, Fink JR, Muzi M, Hanna L, Greco E, et al. ACRIN 6684: assessment of tumor hypoxia in newly diagnosed glioblastoma using 18F-FMISO PET and MRI. Clin Cancer Res 2016;22:5079–86.
32. de Groot J, Penas-Prado M, Alfaro-Munoz K, Hunter K, Pei BL, O'Brien B, et al. Window-of-opportunity clinical trial of pembrolizumab in patients with recurrent glioblastoma reveals predominance of immune-suppressive macrophages. Neuro Oncol 2020;22:539–49.
33. Li W, Graeber MB. The molecular profile of microglia under the influence of glioma. Neuro Oncol 2012;14:958–78.
34. Engler JR, Robinson AE, Smirnov I, Hodgson JG, Berger MS, Gupta N, et al. Increased microglia/macrophage gene expression in a subset of adult and pediatric astrocytomas. PLoS ONE 2012;7:e43339.
35. González-Tablas Pimenta M, Otero Á, Arandia Guzman DA, Pascual-Argente D, Ruíz Martín L, Sousa-Casasnovas P, et al. Tumor cell and immune cell profiles in primary human glioblastoma: impact on patient outcome. Brain Pathol 2021; 31:365–80.
36. Cloughesy TF, Mochizuki AY, Orpilla JR, Hugo W, Lee AH, Davidson TB, et al. Neoadjuvant anti–PD-1 immunotherapy promotes a survival benefit with intratumoral and systemic immune responses in recurrent glioblastoma. Nat Med 2019;25:477–86.